Semiconductor Science and Technology

PAPER

Characterization of ZnO/AlO$_x$/benzene thin-film heterostructures grown through atomic layer deposition/molecular layer deposition

To cite this article: Fabian Krahl *et al* 2020 *Semicond. Sci. Technol.* **36** 025012

View the article online for updates and enhancements.

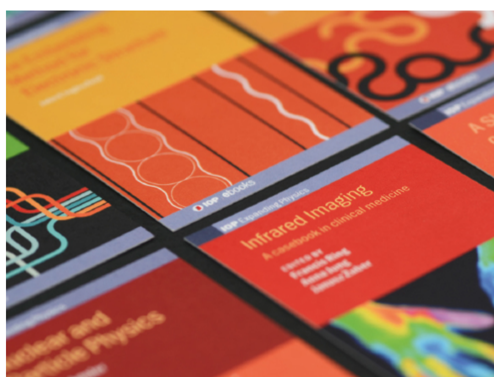

IOP ebooks™

Bringing together innovative digital publishing with leading authors from the global scientific community.

Start exploring the collection–download the first chapter of every title for free.

This content was downloaded from IP address 130.233.92.159 on 26/12/2020 at 07:53

Semicond. Sci. Technol. 36 (2020) 025012 (7pp) https://doi.org/10.1088/1361-6641/abcee2

Characterization of ZnO/AlO$_x$/benzene thin-film heterostructures grown through atomic layer deposition/molecular layer deposition

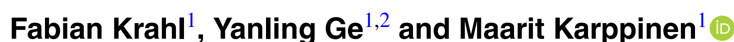
Fabian Krahl[1], **Yanling Ge**[1,2] **and Maarit Karppinen**[1]

[1] Department of Chemistry and Materials Science, School of Chemical Engineering, Aalto University, Espoo, Finland
[2] VTT, Espoo, Finland

E-mail: maarit.karppinen@aalto.fi

Received 4 October 2020, revised 24 November 2020
Accepted for publication 30 November 2020
Published 23 December 2020

Abstract

Multilayer thin-film structures are promising for many future high-tech applications. We investigate the structure of polycrystalline ZnO thin films with sub-nanometer amorphous inorganic (AlO$_x$) and organic (benzene) layers grown by atomic/molecular layer deposition. Small quantities of aluminium are typically introduced in ZnO films for doping, while one of the intended functions of the organic layers is to block thermal conductivity. We apply the AlO$_x$ and benzene layers both simultaneously and separately, and investigate the resultant superlattice films with transmission electron microscopy, x-ray reflectivity and x-ray diffraction measurements. The study reveals that both AlO$_x$ and benzene form distinct layers in the ZnO matrix even down to one atomic/molecular layer. Furthermore, we demonstrate that despite the clear layering, the ZnO grains can penetrate through thin (below ca. 2 nm) benzene and AlO$_x$ layers.

Keywords: atomic layer deposition, molecular layer deposition, inorganic-organic superlattice, ZnO, transmission electron microscopy, x-ray reflectivity

(Some figures may appear in colour only in the online journal)

1. Introduction

Insertion of additional layers in (semiconducting) thin films provides us important means to control various material properties. This is extensively utilized not only for carrier doping, but also to create distinct interfaces for 2D electron gases (e.g. $LaAlO_3/SrTiO_3$ [1, 2]) and for controlling material characteristics such as thermal conductivity (e.g. $SrTiO_3/CaTiO_3$ [3–5]), electrical transport (e.g. ZnO/Al_2O_3 [6, 7]) and optical properties (e.g. Ta_2O_5/Al_2O_3 [8, 9]). Similarly, heterostructures are important for increasing crack resistance and barrier properties (e.g. Al_2O_3/diethylene glycol [10, 11]).

Atomic layer deposition (ALD) is the state-of-the-art thin-film technology in microelectronics [12–14], and an especially powerful deposition technique for layer-engineering owing to its excellent atomic-level layer control due to the stepwise and self-limiting deposition process. Indeed, the layer sequence of different layers has been precisely controlled to grow various heterostructures, including both ternary and quaternary compounds [15, 16] and different superlattice (SL) and nanolaminate structures [17, 18].

There is a counterpart for the ALD technique to deposit organic thin films from gaseous precursors; this technique is called molecular layer deposition (MLD). Most importantly, the two methods, ALD and MLD, can be combined to grow hybrid inorganic-organic thin films for layer-engineered heterostructures. The combined ALD/MLD approach allows the control of the exact thickness of each layer, allowing to combine classical inorganic materials and organic layers in a defined and controlled nanostructure [14, 19, 20].

 © 2020 IOP Publishing Ltd Printed in the UK

Despite the apparent importance of the various thin-film heterostructures, only limited efforts have been made to characterize inorganic-organic multilayer thin films for their interface properties, in particular for the state of the inserted (sub)nanometer thick layers within the host thin-film matrix [21–23]. The open questions include, e.g. how thin can the intermittent layers be before solid-state diffusion becomes an issue, and how well are they separating the matrix material layers. To shed light on these questions we deposited ZnO thin films with AlO_x and benzene intervening layers using ALD/MLD. For ALD, both ZnO and Al_2O_3 are among the prototype materials [24, 25]. In particular, ZnO is composed of earth-abundant and nontoxic elements and has potential as a transparent conductive oxide or thermoelectrics when doped with aluminium [26, 27]. Moreover, also ZnO/Al_2O_3 SL and nanolaminate films have been investigated mostly for their electrical properties [28–30]. Similarly, ZnO/benzene films have been investigated for thermoelectrics, as the inorganic–organic interfaces within the semiconducting ZnO matrix have been shown to work for efficient reduction of thermal conductivity [31–35], as they have extremely high thermal interface resistances (kapitza resistance) [36]. We will demonstrate that even single ALD or MLD cycles on ZnO can lead to distinct layers, but that neither very thin AlO_x nor benzene layers are an effective hindrance to the ZnO grain growth.

2. Methods

2.1. Film deposition

We employed the well-established diethylzinc (DEZ) and water ALD process for growing the ZnO layers [24], and the trimethyl aluminium (TMA) and water ALD process for the AlO_x layers [25, 37]. The benzene layers were deposited by replacing the water precursor in the ZnO process with hydroquinone (HQ) [38, 39]. An advantage with the chosen system is that their deposition temperature windows overlap, making their combination in principle straightforward. The films were deposited on silicon wafers (OKmetic, p-type, cut along the (100) plane) diced into 3 × 3 cm^2 substrates. Prior to deposition they were shortly rinsed with ethanol and dried with an airgun to ensure no dust or organic residue was on the surface.

We deposited the films in a Picosun R-100 reactor at 230 °C and 15 hPa under nitrogen flow (200 sccm), using commercial precursors: DEZ (>52 wt% Zn, Sigma-Aldrich), TMA (97%, Sigma Aldrich), HQ (≥99.5% Reagent plus, Sigma-Aldrich) and deionised water. Nitrogen gas (for purging and transport) was produced in an in-house nitrogen generator (Parker HPN2-5000C-L-230V). All precursors were kept at room temperature in separate containers during the deposition with the exception of HQ which was heated to 150 °C for sublimation. Even at 150 °C, the vapour pressure of HQ is rather low which was compensated by long pulsing times. After each precursor pulse the line and reactor chamber were purged with N_2. The precursor pulse times and corresponding N_2 purge times are given in table 1 for all precursors.

Table 1. Pulse and purge times used in this study.

Precursor	Pulse (s)	Purge (s)
DEZ	0.3	5
H_2O	0.5	5
HQ	15	30
TMA	0.5	5

The samples with both benzene and AlO_x layers were prepared with 51 cycles of DEZ − H_2O followed by x DEZ + HQ cycles, 51 DEZ + H_2O cycles, x TMA + H_2O cycles and 51 DEZ + H_2O cycles; the last four steps were repeated six times. The value of x was either 1 (A6B6) or 10 (A6B6-thick). Additionally, we prepared samples with only AlO_x (A6 and A12) and compared them with previously reported [40] ZnO/benzene samples of the same structure (B6 and B12); in all of those samples x was 1.

2.2. Characterization

X-ray diffraction (XRD) patterns were collected with a Panalytical X'Pert Pro MPD device with Cu–$K_{\alpha1}$ radiation (1.5406 Å) in continuous mode from 2Θ from 5° to 80°. The voltage used to generate the x-rays was 45 kV and the electron flow set to 40 mA. The sample was rotated during the measurement. The grain size (τ) was estimated using the Scherrer formula: $\tau = \frac{K\lambda}{\beta_{2\Theta}\cos(\Theta)}$ from the peak broadening $\beta_{2\Theta}$ (full width at half maximum (FWHM)), shape factor K, wavelength λ, and peak angle Θ [41]. The FWHM of the 002 Si-single crystal substrate peak served as an estimate for instrument broadening and was subtracted from the 002 ZnO FWHM.

X-ray reflectivity (XRR) is a very convenient method to quickly determine not only the thickness of a sample but also the presence of the regular SL structure and its period; for example, in their early study Jensen *et al* showed by XRR distinct layers in their ZnO/Al_2O_3 nanolaminate films [30]. It is based on the reflection of x-rays at the interfaces and the following interference pattern that produces fringes whose distance depends on the distance between the reflecting interfaces, with the SL structures producing 'SL peaks' [41]. These XRR measurements were carried out in a the same XRD equipment except with the following modifications: a stationary sample stage, a copper attenuator and a 0.09 mm anti-scatter slit to reduce the beam intensity and noise at the low measurement angles. The data were analysed using Panalyticals X'Pert XRR program.

Samples for the transmission electron microscopy (TEM) observations were coated with a protective Cu layer (ca. 70 nm) by metal evaporation (Univex 300 Leybold-Heraeus) and then prepared using focused ion beam (FIB) milling with a Ga–Ion source. A 2 μm carbon layer was deposited to avoid damage from ion beam during sample preparation. The ions were accelerated with 30 kV in a JEOL JIB4700

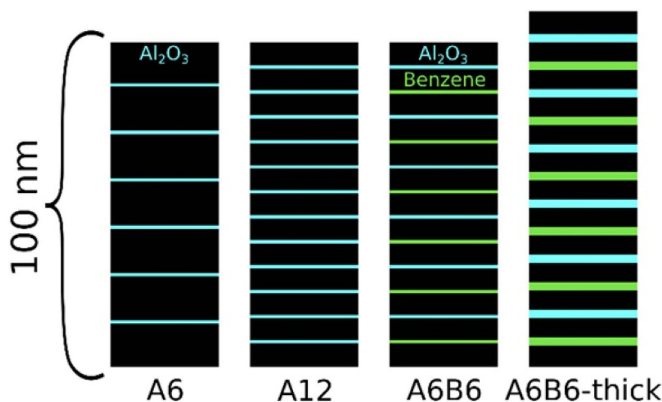

Figure 1. Cross section sketches of the present multi-layered thin-film samples.

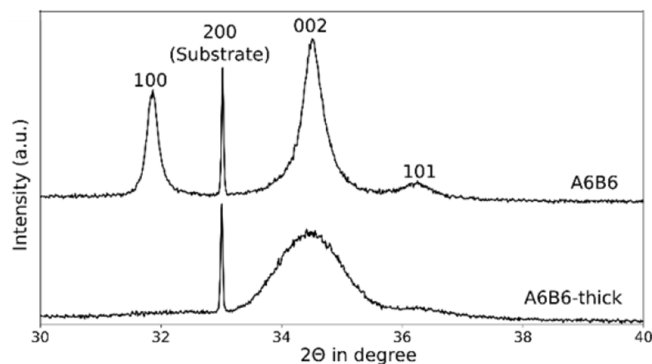

Figure 2. XRD patterns for samples A6B6 and A6B6-thick; the substrate peak is Si (200), all other peaks are from ZnO.

setup with an Omniprobe400 for lift-out of the TEM lamella. The final samples were thinned and polished to ca. 70 nm by gradually decreasing the ion beam voltage and beam size. The images were obtained on a JEOL TEM (JEM2800) with an electron accelerating voltage of 200 kV, using scanning TEM (STEM) mode.

3. Results and discussion

A sketch of the structures of our multilayered thin-film samples is shown in figure 1. Both the total film thickness and the individual layer thicknesses could be accurately determined from the XRR data. We kept the ZnO layers to be equally thick in all samples. Therefore, due to the thicker AlO_x and benzene layers, the sample A6B6-thick is a bit thicker (127 nm) than the other samples which are all around 100 nm thick. For A6B6-thick, the cycle number 10 used to deposit the thicker AlO_x (with 10 TMA + H_2O cycles) and benzene (with 10 DEZ + HQ cycles) layers was chosen on the assumption that the thickness of these layers could be enough to fully separate the ZnO blocks [23].

As will be discussed later in more detail, our TEM and XRR data unambiguously show that both the TMA + H_2O and DEZ + HQ cycles result in distinct layers in all our multilayer thin films (deposited at 230 °C), thus verifying the SL structures sketched in figure 1. From the previous studies for the ALD–ZnO/AlO_x system, it seems that the possible diffusion of aluminium into ZnO may depend on the deposition temperature, and possibly also on other process parameters. Dasgupta *et al* [28] saw an up-shift of the ZnO XRD peaks upon TMA + H_2O cycles for their samples deposited between 140 °C and 220 °C, and Ahn *et al* [29] observed notable Al diffusion when the deposition temperature exceeded 250 °C, while Lee *et al* [42] reported distinct AlO_x layers for their films deposited at 200 °C with single TMA + H_2O cycles with no effect on the lattice parameters of ZnO. It should also be noted that TMA may etch the surface of ZnO during deposition [43, 44]; however, in our samples the effect—if existing—was too small to be observed.

3.1. XRD

Figure 2 shows the XRD patterns for samples A6B6 and A6B6-thick in the 2Θ range of 30°–40°. In this region the three main peaks of ZnO (100, 002 and 101) are present; also visible is a weak silicon substrate peak at 33°. No peaks due to Al_2O_3 could be found (also not outside the shown range), as expected for such a thin and presumably amorphous layers. The same holds true for the Zn–benzene layers. The ZnO layers are polycrystalline with a preference to grow along the *c*-direction; this is in line with previous reports on ALD-grown ZnO films [24, 28, 30, 42, 45]. In the sample A6B6-thick grown with 10 TMA + H_2O cycles and 10 DEZ + HQ cycles ($x = 10$) for each individual barrier layer, the ZnO 002 peak is the only clear peak with the 101 peak being barely visible and the 100 reflection being totally absent.

The grain size estimated from the Scherrer formula is 12 nm in A6B6 which is bigger than the thickness of individual ZnO layers (ca. 8 nm). This is a good indicator that the thin benzene and AlO_x layers are no hard borders for the ZnO growth and that in fact some grains might grow right through these layers. Interestingly, in A6B6-thick the grain size (7 nm) was found to be somewhat smaller, and just below the ZnO-layer thickness. This could be interpreted such that the thicker inserted layers in A6B6-thick work as a strict barrier for the ZnO crystal growth, leading to the lower crystallinity.

3.2. TEM

The observations made from the XRD data could be verified by TEM. First of all, the STEM images of samples A6B6 and A6B6-thick shown in figure 3 reveal clear heterostructures that are in an excellent agreement with the targeted layer sequences; indeed, even our single pulses of TMA lead to clearly distinguishable AlO_x layers (figures 3(a) and (c)).

Moreover, our tentative assumption that the crystal domains can penetrate both the thin benzene and AlO_x layers in A6B6 is especially visible in figure 3(c), where the darker vertical crystallites appear to grow seemingly across any layers. Also, the blocking of the ZnO grain growth at the thicker barrier interfaces in sample A6B6-thick can be confirmed as no grains are seen to clearly penetrate the Zn–benzene or AlO_x layers

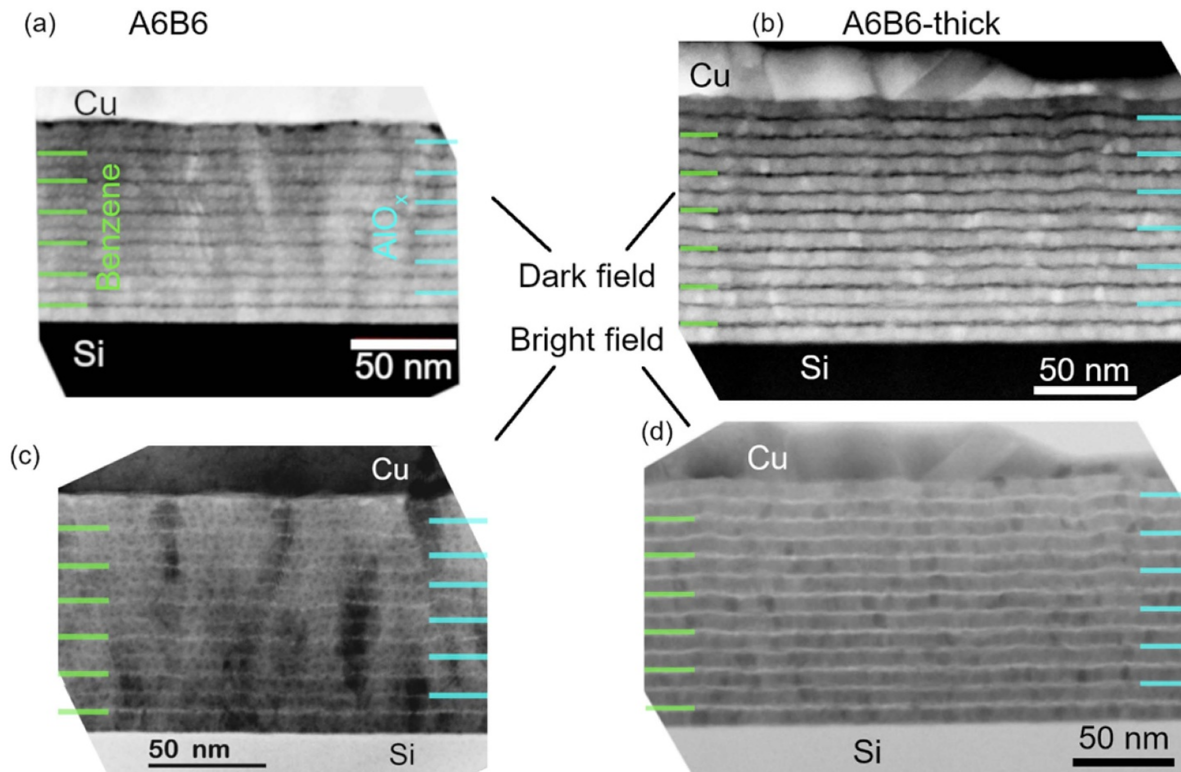

Figure 3. Bright and dark field TEM images of samples A6B6 and A6B6-thick.

grown with $x = 10$ cycles. This is in line with the previous observations made for ZnO films with inserted Zn–benzene layers showing that nine ALD/MLD cycles in minimum were required to block the ZnO penetration [23].

What we now see here for the first time is that the AlO_x layers behave very similar to the benzene layers. This is not straightforwardly expected, given the considerably different chemistries of AlO_x and Zn–benzene moieties. After all benzene is a rather bulky organic molecule and very different from the surrounding ZnO matrix, while AlO_x—even though amorphous—is a metal oxide like ZnO and has a crystalline form (Al_2O_3) crystallizing in the same crystal system. Also, aluminium in small quantities is known to enter the ZnO lattice [26, 27]. However, while the benzene molecules are bulkier they are also not as densely packed and even in an ideal case only every 2nd possible reaction site can be occupied due to steric hindrance [46]. This free space between the benzene molecules could provide pathways for ZnO grains to penetrate the benzene layer and explain why the benzene layers do not seem to be more effective than the AlO_x layers in regards to blocking the ZnO grain growth.

We do see small differences in the electron density of the AlO_x and Zn–benzene layers. Especially in the images from A6B6 this is visible. In the dark field mode where lighter elements appear darker and heavier elements brighter the benzene layers appear much stronger against the ZnO background confirming the lower electron density in these carbon and hydrogen rich layers compared to the Al containing layers (figure 3(a)). Consequently in the bright field mode (lighter elements brighter, heaver elements darker) the benzene layers appear brighter than their Al-rich counterparts (figure 3(c)).

Another noteworthy feature is that the interfaces show a slight 'waviness'. This is small and we are not sure if this is expression of the inserted AlO_x and Zn–benzene layers growing over a slightly rugged polycrystalline ZnO surface, 'smoothening' the film in the process, as such an effect has been mentioned in literature [47, 48]. Another plausible explanation could be a post-deposition smearing that could happen have happened during the FIB cutting.

3.3. XRR

Simulating the XRR patterns yielded the film thicknesses at 107 and 124 nm for the two heterolayered samples, A6B6 and A6B6-thick, respectively, and an interface roughness of around 1 nm for both. All these values match well with the TEM data (figure 3). The XRR patterns also show clear SL peaks, marked with arrows in figure 4; this nicely highlights the capability of XRR to detect SL-type heterostructures. Not surprisingly, the SL peaks are much more pronounced for A6B6-thick reflecting the thicker intermittent layers and the better-defined interfaces. Nevertheless, the SL peaks can be found in all samples. In direct comparison, the B6 and B12 samples with 6 or 12 Zn–benzene layers, respectively (and previously reported [40]), show slightly more pronounced SL peaks than the A6 and A12 samples with 6 or 12 AlO_x layers. We think this is due to the ZnO/benzene having a bigger difference in electron density than the ZnO/AlO_x boundary as

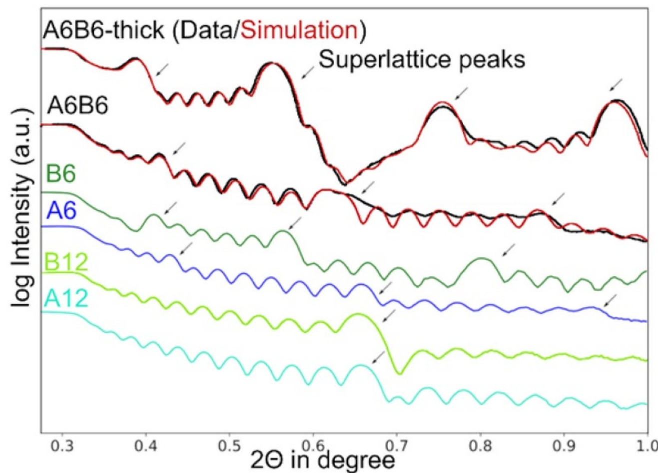

Figure 4. XRR patterns for samples A6B6 and A6B6-thick, and also for A6, B6, A12 and B12 as comparison; B6 and B12 patterns are from samples reported in [40] .

Table 2. Total film and individual layer thicknesses obtained from XRR simulations and TEM images.

Thickness (nm)	From XRR	From TEM
ZnO layers in A6B6	8 ± 1	6 ± 2
ZnO layers in A6B6-thick	7 ± 1	7 ± 2
AlO_x in A6B6	0.1 ± 1	1.3 ± 2
AlO_x in A6B6-thick	2.5 ± 1	1.7 ± 2
Benzene in A6B6	0.3 ± 1	1.8 ± 2
Zn–benzene in A6B6-thick	3 ± 1	1.7 ± 2
Total film A6B6	106 ± 5	102 ± 2
Total film A6B6-thick	124 ± 5	119 ± 2

was already indicated in the slightly stronger contrast of the ZnO/benzene boundary in the TEM images. The overall density for all films was between 5.5 and 5.6 g cm^{-3} and, within the error limits, essentially the same as for bulk ZnO (5.6 g cm^{-3} [49]). The excellent agreement between the XRR and TEM data is a promising observation, as XRR is a much quicker and cost-efficient technique to perform in routine work.

It is interesting to note that XRR is able to distinguish between the two different barrier layers as the measured pattern clearly shows 6 repeating subunits and not 12 for A6B6 and A6B6-thick. In figure 4 these samples are compared with samples that only have benzene or AlO_x interface layers but not both. The similarity of A6B6 with samples that have 6 AlO_x or benzene layers (A6 and B6 in figure 4) is striking and very different from samples that have 12 AlO_x or benzene layers (A12 and B12) despite the total number of interface layers in A6B6 equalling that of A12 and B12.

Table 2 shows the individual layer thicknesses obtained from analysing the electron microscope images and the simulations of the XRR curves; in overall the results are very similar, the biggest difference being in the individual thicknesses of AlO_x and benzene layers, which also have the biggest relative errors. In the XRR simulation this error comes from the fact that the fringes represent the overall film thickness and changes below 1 nm, e.g. AlO_x would result in very little change in the overall thickness of the film, so really the thicknesses of these very thin layers must be taken with great care. In the electron microscope images the biggest error comes from the benzene and AlO_x layers not being completely flat, the slight waviness mentioned before and seen in figure 3 is also present in the beam direction (perpendicular to the picture plane) and leads to a 'smearing' of the layers making the thin layers in the pictures appear bigger than they might really be, the same is true for the surface (capped with copper).

4. Conclusions

Deposition of AlO_x layers with TMA + H_2O ALD cycles and Zn–benzene layers with DEZ + HQ ALD/MLD cycles within a ZnO thin film at 230 °C leads to a strictly multilayered thin-film structure. Both of the inserted materials can be clearly distinguished from the surrounding polycrystalline ZnO matrix. This is shown in the XRR patterns and depictured on the TEM images. Most excitingly, XRR clearly detects SL structures with six repetitions for films with 6 + 6 alternate AlO_x and Zn–benzene layers.

Regarding the efficiency to block the ZnO grain growth, no clear difference between the AlO_x and Zn–benzene layers was seen, despite their different electron densities (seen by both XRR and TEM) and chemistry features. In both cases, ZnO was shown to grow through the very thin interfaces grown with only ALD or ALD/MLD cycle, whereas using ten deposition cycles effectively hindered the ZnO-grain growth through the layer. This was seen from the TEM images and also revealed from the grain size analysis with XRD, showing a reduction in average grain size with thicker interface layers.

The present study has thus demonstrated the capability of ALD/MLD in engineering well-defined multilayered heterostructures of chemically different components, like AlO_x and benzene in a ZnO matrix down to monoatomic/molecular layers within the same sample; even with only one single precursor pulse the layering stays intact and is clearly visible.

Acknowledgments

We acknowledge the funding from the European Research Council under the European Union's Seventh Framework Programme (FP/2007-2013)/ERC Advanced Grant Agreement (339478) and Academy of Finland (296299). This work made use of the RawMatTERS Finland Infrastructure (RAMI) and OtaNano—Nanomicroscopy Center (Aalto-NMC) at Aalto University.

ORCID iD

Maarit Karppinen https://orcid.org/0000-0003-1091-1169

References

[1] Ohtomo A and Hwang H Y 2004 A high-mobility electron gas at the $LaAlO_3/SrTiO_3$ heterointerface *Nature* **427** 423–6
[2] Nakagawa N, Hwang H Y and Muller D A 2006 Why some interfaces cannot be sharp *Nat. Mater.* **5** 204–9
[3] Ravichandran J *et al* 2014 Crossover from incoherent to coherent phonon scattering in epitaxial oxide superlattices *Nat. Mater.* **13** 168–72
[4] Cahill D G, Bullen A and Lee S-M 2000 Interface thermal conductance and the thermal conductivity of multilayer thin films *HTHP* **32** 135–42
[5] Hicks L D and Dresselhaus M S 1993 Effect of quantum-well structures on the thermoelectric figure of merit *Phys. Rev.* B **47** 12727–31
[6] Ohtomo A and Tsukazaki A 2005 Pulsed laser deposition of thin films and superlattices based on ZnO *Semicond. Sci. Technol.* **20** S1–S12
[7] Gong Y-P, Li A-D, Li X-F, Li H, Zhai H-F and Wu D 2010 Impact of the Al/Hf ratio on the electrical properties and band alignments of atomic-layer-deposited HfO_2/Al_2O_3 on S-passivated GaAs substrates *Semicond. Sci. Technol.* **25** 055012
[8] Szeghalmi A, Senz S, Bretschneider M, Gösele U and Knez M 2009 All dielectric hard x-ray mirror by atomic layer deposition *Appl. Phys. Lett.* **94** 133111
[9] Färm E, Mehravar S, Kieu K, Peyghambarian N, Ritala M, Leskelä M and Kemell M 2019 Controlling the refractive index and third-order nonlinearity of polyimide/Ta_2O_5 nanolaminates for optical applications *J. Vac. Sci. Technol.* A **37** 060908
[10] Vähä-Nissi M, Sundberg P, Kauppi E, Hirvikorpi T, Sievänen J, Sood A, Karppinen M and Harlin A 2012 Barrier properties of Al_2O_3 and alucone coatings and nanolaminates on flexible biopolymer films *Thin Solid Films* **520** 6780–5
[11] Graff G L, Williford R E and Burrows P E 2004 Mechanisms of vapor permeation through multilayer barrier films: lag time versus equilibrium permeation *J. Appl. Phys.* **96** 1840–9
[12] Suntola T 1989 Atomic layer epitaxy *Mater. Sci.* **4** 261–312
[13] Leskelä M and Ritala M 2002 Atomic layer deposition (ALD): from precursors to thin film structures *Thin Solid Films* **409** 138–46
[14] George S M 2010 Atomic layer deposition: an overview *Chem. Rev.* **110** 111–31
[15] Mackus A J M, Schneider J R, MacIsaac C, Baker J G and Bent S F 2019 Synthesis of doped, ternary, and quaternary materials by atomic layer deposition: a review *Chem. Mater.* **31** 1142–83
[16] Larsson F, Stolt L, Hultqvist A, Edoff M, Keller J and Törndahl T 2020 Atomic layer deposition of ternary compounds on Cu(In,Ga)Se_2: an in situ quartz crystal microbalance study *ACS Appl. Energy Mater.* **3** 7208–15
[17] Chen X and Baumgart H 2020 Advances in atomic layer deposition (ALD) nanolaminate synthesis of thermoelectric films in porous templates for improved Seebeck coefficient *Materials* **13** 1283
[18] Wiegand C W, Faust R, Meinhardt A, Blick R H, Zierold R and Nielsch K 2018 Understanding the growth mechanisms of multilayered systems in atomic layer deposition process *Chem. Mater.* **30** 1971–9
[19] Sundberg P and Karppinen M 2014 Organic and inorganic–organic thin film structures by molecular layer deposition: a review *Beilstein J. Nanotechnol.* **5** 1104–36
[20] Nilsen O, Klepper K, Nielsen H and Fjellvåg H 2008 Deposition of organic-inorganic hybrid materials by atomic layer deposition *ECS Trans.* **16** 3–14
[21] Lee B H, Ryu M K, Choi S-Y, Lee K-H, Im S and Sung M M 2007 Rapid vapor-phase fabrication of organic−inorganic hybrid superlattices with monolayer precision *J. Am. Chem. Soc.* **129** 16034–41
[22] Choudhury D and Sarkar S K 2014 The ALD-MLD growth of a ZnO-zincone heterostructure *Chem. Vap. Depos.* **20** 130–7
[23] Niemelä J-P, Aghaee M, Kessels W M M E, Creatore M and Verheijen M A 2019 Transition in layer structure of atomic/molecular layer deposited ZnO-zincone multilayers *J. Vac. Sci. Technol.* A **37** 040602
[24] Tynell T and Karppinen M 2014 Atomic layer deposition of ZnO: a review *Semicond. Sci. Technol.* **29** 043001
[25] Puurunen R L 2005 Surface chemistry of atomic layer deposition: a case study for the trimethylaluminum/water process *J. Appl. Phys.* **97** 121301
[26] Özgür Ü, Alivov Ya I, Liu C, Teke A, Reshchikov M A, Doğan S, Avrutin V, Cho S-J and Morkoç H 2005 A comprehensive review of ZnO materials and devices *J. Appl. Phys.* **98** 041301–1–103
[27] Klingshirn C F, Waag A, Geurts J, Hoffmann A and Meyer B K 2010 *Zinc Oxide* (Berlin: Springer)
[28] Dasgupta N P, Neubert S, Lee W, Trejo O, Lee J-R and Prinz F B 2010 Atomic layer deposition of Al-doped ZnO films: effect of grain orientation on conductivity *Chem. Mater.* **22** 4769–75
[29] Ahn C H, Kim S H, Kim Y K, Lee H S and Cho H K 2015 Effect of post-annealing temperatures on thin-film transistors with ZnO/Al_2O_3 superlattice channels *Thin Solid Films* **584** 336–40
[30] Jensen J M, Oelkers A B, Toivola R, Johnson D C, Elam J W and George S M 2002 X-ray reflectivity characterization of ZnO/Al_2O_3 multilayers prepared by atomic layer deposition *Chem. Mater.* **14** 2276–82
[31] Tynell T, Giri A, Gaskins J, Hopkins P E, Mele P, Miyazaki K and Karppinen M 2014 Efficiently suppressed thermal conductivity in ZnO thin films via periodic introduction of organic layers *J. Mater. Chem.* A **2** 12150–2
[32] Giri A, Niemelä J-P, Tynell T, Gaskins J T, Donovan B F, Karppinen M and Hopkins P E 2016 Heat-transport mechanisms in molecular building blocks of inorganic/organic hybrid superlattices *Phys. Rev.* B **93** 115310
[33] Krahl F, Giri A, Tomko J A, Tynell T, Hopkins P E and Karppinen M 2018 Thermal conductivity reduction at inorganic–organic interfaces: from regular superlattices to irregular gradient layer sequences *Adv. Mater. Interfaces* **5** 1701692
[34] Tynell T, Terasaki I, Yamauchi H and Karppinen M 2013 Thermoelectric characteristics of (Zn, Al)O/hydroquinone superlattices *J. Mater. Chem.* A **1** 13619–24
[35] Tynell T and Karppinen M 2014 ZnO:hydroquinone superlattice structures fabricated by atomic/molecular layer deposition *Thin Solid Films* **551** 23–26
[36] Giri A and Hopkins P E A 2019 Review of experimental and computational advances in thermal boundary conductance and nanoscale thermal transport across solid interfaces *Adv. Funct. Mater.* **0** 1903857
[37] George S M, Ott A W and Klaus J W 1996 Surface chemistry for atomic layer growth *J. Phys. Chem.* **100** 13121–31
[38] Yoon B, Lee B H and George S M 2012 Highly conductive and transparent hybrid organic–inorganic zincone thin films using atomic and molecular layer deposition *J. Phys. Chem.* C **116** 24784–91
[39] Yoon B, Lee Y, Derk A, Musgrave C and George S 2011 Molecular layer deposition of conductive hybrid organic-inorganic thin films using diethylzinc and hydroquinone *ECS Trans.* **33** 191–5
[40] Krahl F, Hoque S B, Giri A, Sederholm L, Hopkins P E and Karppinen M 2020 Experimental control and statistical

analysis of thermal conductivity in ZnO-benzene multilayer thin films *J. Phys. Chem.* C **124** 24731–9

[41] Birkholz M 2006 *Thin Film Analysis by X-Ray Scattering* (Weinheim: Wiley)

[42] Lee D-J, Kim H-M, Kwon J-Y, Choi H, Kim S-H and Kim K-B 2011 Structural and electrical properties of atomic layer deposited Al-doped ZnO films *Adv. Funct. Mater.* **21** 448–55

[43] Elam J W and George S M 2003 Growth of ZnO/Al_2O_3 alloy films using atomic layer deposition techniques *Chem. Mater.* **15** 1020–8

[44] Zywotko D R and George S M 2017 Thermal atomic layer etching of ZnO by a 'conversion-etch' mechanism using sequential exposures of hydrogen fluoride and trimethylaluminum *Chem. Mater.* **29** 1183–91

[45] Ghiyasi R, Tewari G C and Karppinen M 2020 Organic-component dependent crystal orientation and electrical transport properties in ALD/MLD grown ZnO-organic superlattices *J. Phys. Chem.* C **124** 13765–70

[46] Karttunen A J, Tynell T and Karppinen M 2015 Atomic-level structural and electronic properties of hybrid inorganic-organic ZnO:hydroquinone superlattices fabricated by ALD/MLD *J. Phys. Chem.* C **119** 13105–14

[47] Banerjee P, Lee W-J, Bae K-R, Lee S B and Rubloff G W 2010 Structural, electrical, and optical properties of atomic layer deposition Al-doped ZnO films *J. Appl. Phys.* **108** 043504

[48] Geng Y, Guo L, Xu S-S, Sun Q-Q, Ding S-J, Lu H-L and Zhang D W 2011 Influence of Al doping on the properties of ZnO thin films grown by atomic layer deposition *J. Phys. Chem.* C **115** 12317–21

[49] Haynes W M (ed) 2011 *CRC Handbook of Chemistry and Physics* (Boca Raton, FL: CRC Press)